Available online at www.sciencedirect.com
SCIENCE DIRECT
Journal of Catalysis 242 (2006) 16–25
JOURNAL OF CATALYSIS
www.elsevier.com/locate/jcat

# An operando Raman study of structure and reactivity of alumina-supported molybdenum oxide catalysts for the oxidative dehydrogenation of ethane

A. Christodoulakis [a], E. Heracleous [b], A.A. Lemonidou [b], S. Boghosian [a,*]

[a] *Department of Chemical Engineering, University of Patras and Institute of Chemical Engineering, Foundation of Research and Technology-Hellas (FORTH/ICE-HT), 26500 Patras, Greece*
[b] *Department of Chemical Engineering, University of Thessaloniki and Chemical Process Engineering Research Institute, CERTH/CPERI, PO Box 1517, GR-54006 Thessaloniki, Greece*

Received 16 December 2005; revised 12 May 2006; accepted 22 May 2006

Available online 23 June 2006

**Abstract**

The structural and catalytic properties of supported $MoO_3/Al_2O_3$ catalysts with Mo surface densities, $n_s$, in the range 1.1–12.5 Mo/nm$^2$ were studied for the oxidative dehydrogenation of ethane by in situ Raman spectroscopy with simultaneous catalytic measurements at temperatures of 400–550 °C. Isolated mono-molybdates ($MoO_4$) and polymolybdates are formed at various proportions (depending on the loading) on the catalyst surface under dehydrated conditions; bulk $Al_2(MoO_4)_3$ crystals are formed at $n_s$ exceeding the monolayer. Under reactive environment ($C_2H_6/O_2$), the Raman features attributed to Mo=O and Mo–O–Mo modes appear to be perturbed, indicating that surface $MoO_x$ species are reduced to lower valence states. The combined information on catalyst structure under reaction conditions and catalytic data shows a concurrence between the trends for activity per Mo (turnover frequency [TOF]) and for the number of Mo–O–Al bonds per Mo as a function of $n_s$. The catalytic activity is related to the anchoring Mo–O–support bonds. Structure–activity/selectivity relations are derived and discussed.


*Keywords:* In situ Raman spectra; Ethane ODH; Molecular structure; Molybdena active sites; $MoO_3/Al_2O_3$ catalysts; Anchoring bonds

## 1. Introduction

The demand for olefins remains a challenge for the refining and petrochemical industry. The classical commercial processes applied for the production of olefins are energy-intensive, and more economic sources are sought [1,2]. The catalytic dehydrogenation of alkanes is an attractive route for the synthesis of alkenes from the cheaper corresponding alkanes. Both dehydrogenation (DH) [3] and oxidative dehydrogenation (ODH) [4–7] reactions can be used, with often-comparable yields in olefins and losses in $CO_x$. In the presence of an oxidant (e.g., $O_2$), the process becomes exothermic, which can result in a control of carbon deposition that would otherwise necessitate frequent catalyst regeneration. However, combustion pathways to $CO_x$ limit alkene yields, especially at high alkane conversions. Therefore, the design of selective catalysts appears critical for the efficiency of the ODH process.

Supported $MoO_3$ catalysts are important catalytic systems for the oxidative dehydrogenation of light alkanes [8–10]. The efficient activation of the reactants is related to the local structure, the distribution of metal oxide species on the support surface, and parameters related to the preparation procedures of the catalysts [11–13].

Raman spectroscopy is among the most powerful tools for studying catalytic materials and surfaces under in situ conditions [14–19]. It can provide information on the molecular structure of the surface metal oxide species by probing the vibrational properties of metal–oxygen bonds. The structures of $MoO_3$-supported catalysts at dehydrated conditions evolve from isolated monomers to larger polymolybdates, for submonolayer coverages of the support. For coverages exceeding the monolayer, bulk $MoO_3$ and/or $Al_2(MoO_4)_3$ crystals have been reported to form on $Al_2O_3$, depending on the Mo surface density and the sample preparation conditions [20,21]. The relative concentrations of the various surface $MoO_x$ species depend

* Corresponding author.
*E-mail address:* bogosian@iceht.forth.gr (S. Boghosian).

0021-9517/$ – see front matter 
doi:10.1016/j.jcat.2006.05.024

on the specific metal oxide support, the Mo surface density, and the calcination temperature of the sample.

The need for a deeper understanding of the nature and the function of catalytically active species during a catalytic process has led to a dramatic increase in the number of in situ Raman characterization studies [16]. The urge for establishing structure–activity/selectivity relationships has led to the development of spectroscopic instrumentation, allowing monitoring of catalytic systems with simultaneous on-line product analysis under actual reaction conditions. The above strategy has been termed *operando* spectroscopy. Many recent publications have stressed the potential of this strategy and its value in catalysis research [22–26].

This work focuses on the investigation of supported $MoO_3/Al_2O_3$ catalysts for ethane ODH by means of *operando* Raman spectroscopy. In situ Raman spectra were recorded at temperatures of 400–550 °C with simultaneous collection of catalytic activity data from the same sample. The effect of catalyst composition, temperature, gas atmosphere, and reactant residence time on both Raman spectra and catalytic efficiency was studied. The data were used to derive structure–activity/selectivity relationships for ethane ODH over $MoO_3/Al_2O_3$-supported catalysts.

## 2. Experimental

### 2.1. Catalyst preparation and characterization

Supported $MoO_3/Al_2O_3$ catalysts were prepared by wet impregnation of $\gamma$-$Al_2O_3$ (Engelhard; surface area [SA] = 183.9 $m^2/g$). Before impregnation, the support was crushed and sieved to a particle size of 106–180 μm. Ammonium heptamolybdate [$(NH_4)_6Mo_7O_{24}\cdot 4H_2O$, Fisher] was used as the Mo precursor. To ensure full dissolution of the precursor to water, the solution (0.01–0.06 $g/cm^3$, pH = 5) was heated at 40 °C. The weight loading of $MoO_3$ varied between 5 and 30%. Impregnation of the dry alumina particles with the Mo precursor solution was conducted at 70 °C for 1 h in a rotary evaporator. After impregnation, the solvent was removed by evaporation at 70 °C under reduced pressure (200 mmHg) for 45 min. The resulting solid was dried overnight at 120 °C and calcined in synthetic air (flow, 50 $cm^3/min$) at 650 °C for 6 h in a muffle furnace. The catalysts are denoted by *x*MoAl, where *x* indicates the nominal wt% $MoO_3$ loading of the catalyst.

X-ray crystallography characterization for determining the Mo content, specific SAs, and crystalline phases of the samples has been described elsewhere [8]. The catalyst characteristics are summarized in Table 1.

### 2.2. In situ Raman spectroscopy with simultaneous gas chromatography analysis

An appropriate homemade in situ Raman cell was designed and constructed for the simultaneous monitoring of Raman spectra and catalytic activity of the studied catalysts (Fig. 1). The reactor cell, which had a gas inlet and a gas outlet as well as an entrance to accommodate a thermocouple sheath, was made of quartz tubing (6 mm o.d.; 4 mm i.d. and 10 mm o.d.; 8 mm i.d. for the central larger part; see Fig. 1) and had

Table 1
Properties of the catalysts

| Catalyst | wt% $MoO_3$ | | SA ($m^2/g$) | Surface density ($Mo/nm^2$) | Crystalline phases |
|---|---|---|---|---|---|
| | Nominal | ICP analysis | | | |
| 5MoAl | 5 | 4.8 | 186 | 1.1 | $\gamma$-$Al_2O_3$ |
| 10MoAl | 10 | 9.5 | 178 | 2.3 | $\gamma$-$Al_2O_3$ |
| 15MoAl | 15 | 14.8 | 161 | 3.9 | $\gamma$-$Al_2O_3$ |
| 20MoAl | 20 | 20.3 | 124 | 6.7 | $\gamma$-$Al_2O_3$, $Al_2(MoO_4)_3$ |
| 30MoAl | 30 | 29.3 | 100 | 12.5 | $\gamma$-$Al_2O_3$, $Al_2(MoO_4)_3$ |

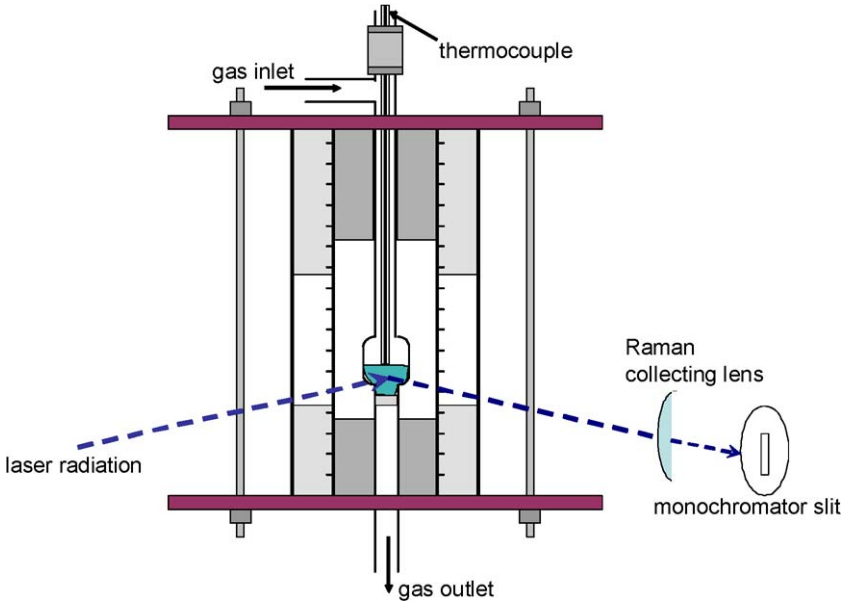


Fig. 1. Home made Raman cell for *operando* Raman—GC measurements.

a quartz frit for holding the catalysts in a fixed bed (particle size, 100–180 μm). The reactor cell was mounted in vertical position inside a double-walled quartz-glass transparent tube furnace (Fig. 1) mounted on a $xyz$ plate allowing it to be positioned on the optical table. The inner furnace tube is kanthal wire-wound for heating the reactor. Temperature was controlled and measured by a thermocouple inserted in the quartz sheath in contact with the catalyst bed.

The 488-nm line of a Spectra Physics Stabilite 2017 $Ar^+$ laser was used for recording of the Raman spectra, operated at a power level of 40 mW at the sample. To reduce irradiance on samples, the laser light was "dispersed" by (slightly) defocussing the incident beam. The scattered light was collected at 90° (horizontal scattering plane), analyzed with a 0.85 Spex 1403 double spectrometer, and detected by a −20 °C cooled RCA PMT equipped with EG&G photon counting electronics.

In situ Raman spectra under oxidizing conditions at temperatures of 420–540 °C were performed under flowing $O_2$ (99.999%) at a 15 $cm^3$/min flow rate controlled by electronic mass flowmeters. Before recording the spectra, catalysts were maintained at each temperature for at least 1 h under flowing $O_2$ to ensure full oxidation. For the *operando* Raman–gas chromatography (GC) measurements during steady-state ethane ODH conditions, a flow of a reactant gas mixture consisting of 5.6% $C_2H_6$/5.6% $O_2$ balanced in He was admitted in the Raman reactor after treatment in $O_2$ at 550 °C. The weight of the catalysts and the total flow rate of the reactants were appropriately adjusted to attain different values of residence time, expressed hereinafter by the $W/F$ ratio ($W$, catalyst weight; $F$, total gas flow). Typically, 280 mg of catalyst was examined under reaction conditions at a total feed flow rate of 60 $cm^3$/min ($W/F = 0.28$ g s/$cm^3$) in the temperature range 420–540 °C. In a second series of measurements, the reaction temperature was kept constant at 540 °C, and the effect of bed residence time on catalytic performance was explored by varying either the catalyst weight (150–300 mg) or the total flow rate (50–200 $cm^3$/min), resulting in $W/F$ values in the range of 0.05–0.67 g s/$cm^3$. In both series of measurements, before changing the temperature or the residence time ($W/F$), the catalysts were reoxidized in pure flowing $O_2$ (15 $cm^3$/min) for at least 1 h at 550 °C.

The reactor effluent was analyzed by on-line GC using a Schimadju 14B with two packed columns (Porapak Q and Molecular Sieve 5A) in a series or bypass configuration, along with a thermal conductivity detector (TCD). Blank runs with no catalyst in the bed were also performed to check the case of gas-phase reaction contributions, and ethane conversion was <1% at the maximum temperature under the measurement conditions.

## 3. Results and discussion

### 3.1. In situ Raman spectra of catalysts under $O_2$

Fig. 2 shows the in situ Raman spectra under $O_2$ conditions obtained for all catalyst samples as a function of molybdena loading at 540 °C. All spectra were normalized with respect to

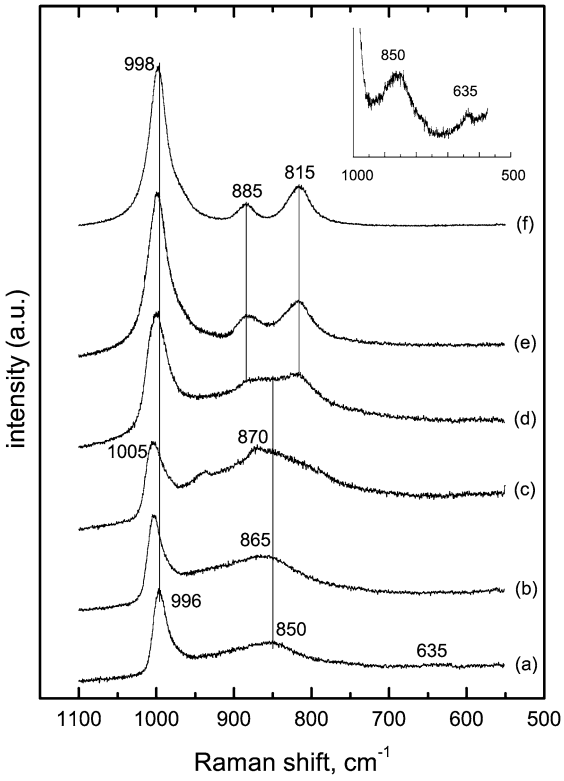


Fig. 2. In situ Raman spectra of oxidized catalysts obtained under flowing $O_2$ at 540 °C: (a) 5MoAl; (b) 10MoAl; (c) 15MoAl; (d) 20MoAl; (e) 30MoAl; and (f) $Al_2(MoO_4)_3$. Inset: Magnification of the 550–1000 $cm^{-1}$ region obtained from a self-supported 5MoAl wafer under $O_2$ at 540 °C. Laser wavelength, $\lambda_0 = 488.0$ nm; laser power, $w = 25$ mW; scan rate, sr = 0.07–0.2 $cm^{-1}$/s; time constant, $\tau = 1$–7 s; spectral slit width, ssw = 8 $cm^{-1}$.

the 604-$cm^{-1}$ Raman peak due to $SiO_2$ (quartz reactor wall material). After normalization, the spectrum of vitreous silica (recorded by obtaining a Raman spectrum of the empty reactor cell at the same optical geometry) was subtracted from the normalized spectra of the catalysts. In situ Raman spectra were also recorded using an alternative cell construction [17,19] (not suitable for consideration as a differential reactor) in which the catalyst sample is in the form of a self-supported pressed wafer and there is no contact with window materials, to ensure that the subtraction process performed when using the cell shown in Fig. 1 does not affect the resulting spectra. The limit for monolayer coverage of the $Al_2O_3$ support is reportedly ∼5 Mo/$nm^2$, as determined experimentally [27] and from geometrical considerations [28]. At loadings up to 6.7 Mo/$nm^2$ (i.e., below or near the monolayer limit [spectra a–d in Fig. 2]), a well-defined Raman band in the Mo=O terminal stretching region at ∼1000 $cm^{-1}$ and a broad band in the 850–870 $cm^{-1}$ region due to Mo–O–Mo functionalities [29–32] are observed, in agreement with previously reported Raman data [32–34]. With increasing loading, the Mo=O band is blue-shifted from 996 to 1005 $cm^{-1}$, and the Mo–O–Mo band is blue-shifted from 850 to 870 $cm^{-1}$ and its intensity is gradually increased relative to the Mo=O band. Additionally, the spectrum of the 5MoAl sample with the lowest loading (1.1 Mo/$nm^2$) exhibits a weak feature at ∼635 $cm^{-1}$, also observed previously [33]. The inset in Fig. 2 shows an enlargement of the 500–1000 $cm^{-1}$ region for the

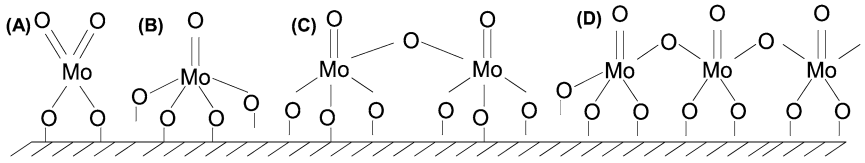


Fig. 3. Possible molecular configurations for $MoO_x$ surface species on $Al_2O_3$: (A) tetrahedrally coordinated $MoO_4$ species, (B) dimeric surface species with distorted octahedral coordination, (C) polymeric $MoO_x$ species, octahedrally coordinated.

Table 2
Raman stretching frequencies from reference compounds (from Ref. [36])

| Compound | $\nu_2(A_1)$ (symmetric M=O) | $\nu_8(B_2)$ (antisymmetric M=O) weak in Raman |
|---|---|---|
| $[O_2VF_2]^-$ | 970 | 962 |
| $[O_2VCl_2]^-$ | 970 | 959 |
| $O_2CrF_2$ | 1006 | 1016 |
| $O_2CrCl_2$ | 995 | 1002 |
| $O_2MoBr_2$ | 995 | 970 |
| $[O_2MoS_2]^{2-}$ | 819 | 801 |

5MoAl sample obtained from a pressed self-supported wafer under $O_2$ at 540 °C, that is, without the need to subtract the scattering from the quartz wall of the reactor cell. When loading slightly exceeds the monolayer coverage (20MoAl, $n_s = 6.7$ Mo/nm$^2$), bands due to bulk $Al_2(MoO_4)_3$ at 815, 885, and 998 cm$^{-1}$ emerge in the spectrum (Fig. 2d) and partly obscure the Mo–O–Mo modes in the 750–950 cm$^{-1}$ region. However, because the Raman cross-section is much higher for crystalline $Al_2(MoO_4)_3$ than for dispersed surface $MoO_x$, it is evident that most of the Mo is highly dispersed on the alumina surface. With further increase in loading, the $Al_2(MoO_4)_3$ bands dominate in the spectrum of 30MoAl ($n_s = 12.5$ Mo/nm$^2$) shown in Fig. 2e. The spectrum of bulk $Al_2(MoO_4)_3$ is included in Fig. 2f for comparison. The observed formation of $Al_2(MoO_4)_3$ for samples with $n_s$ exceeding the monolayer (20 and 30MoAl) can be due to the high calcination temperature (650 °C) as pointed out earlier [20].

Previously [33], it has been shown that under dehydrated conditions the predominant species at the surface of $MoO_3/Al_2O_3$ catalysts with low loadings are isolated monomolybdates in distorted tetrahedral coordination with two terminal Mo=O and two bridging Mo–O–support bonds. Dioxo transition metal–oxygen units possess symmetric and antisymmetric M=O modes, the splitting of which is in the range 10–30 cm$^{-1}$ (see Table 2) [35,36]. Therefore, the lack of symmetry in the shape of the 996 cm$^{-1}$ band indicates the existence of overlapping symmetric and antisymmetric Mo=O modes within dioxo O=Mo=O units. However, a monooxo configuration with four anchoring Mo–O–support bonds cannot be excluded [29,37].

The Raman features observed can be assigned to the following surface $MoO_x$ species: isolated distorted tetrahedral dioxo molybdates with two Mo=O and two Mo–O–support bonds (Fig. 3A), isolated monooxo O=Mo–(O–Al)$_4$ with four anchoring bonds (Fig. 3B) and $MoO_x$ species possessing Mo–O–Mo bridges (models C and D in Fig. 3), which give rise to the 850–870 cm$^{-1}$ band due to Mo–O–Mo functionalities [29–32]. Terminal Mo=O bonds associated to polymolybdates contribute also to the 996 cm$^{-1}$ band [34] as it is known that Mo=O modes within tetrahedral/octahedral and monomeric/polymeric Mo surface species usually overlap [29,33,38]. A surface dimeric $MoO_x$ species with one short Mo=O bond and three anchoring Mo–O–support bonds per Mo atom, with a coordination number (CN) for Mo of 5, would result in the configuration shown in Fig. 3C. Such a model was also proposed for higher $MoO_3$ loadings on $ZrO_2$ [34]. The 635 cm$^{-1}$ weak band (see inset in Fig. 2) can be due to Mo–O–support anchoring bonds that are expected to appear at this spectral region [14].

The gradual increase of the 850–870 cm$^{-1}$ band intensity relative to the ∼1000 cm$^{-1}$ Mo=O band indicates a higher degree of polymerization for the dispersed $MoO_x$ chains as loading increases. This is in agreement with the increase in the number of Mo–O–Mo bridges *per* Mo=O with increasing degree of polymerization. For example (see Fig. 3), there are 0.5 bridges per Mo=O in a dimeric species and 0.67 bridges per Mo=O in a trimeric species and this effect justifies a faster enhancement of the 850–870 cm$^{-1}$ band intensity (due to Mo–O–Mo) compared to the intensity of the 1005 cm$^{-1}$ (Mo=O) with increase in loading. The broadness of the 850–870 cm$^{-1}$ band suggests a wide distribution of Mo–O–Mo bond distances within polymeric $MoO_x$ species [32]. Furthermore, the blue shift of Mo–O–Mo modes (i.e., from 850 cm$^{-1}$ in 5MoAl to ∼870 cm$^{-1}$ with increasing loading) indicates strengthening of the Mo–O bonds along Mo–O–Mo bridges and subsequent weakening of the Mo–O bonds along Mo–O–Al anchors.

The consistency of the Raman assignments can be checked using the following correlations between the M–O Raman stretching frequencies and the corresponding M–O bond lengths and Pauling bond strengths [40]:

$$\nu = 32{,}895 \exp(-2.073R) \tag{1}$$

and

$$s = (R/1.882)^{-6}, \tag{2}$$

where $\nu$ is the Mo–O Raman stretching frequency (cm$^{-1}$), $R$ the corresponding bond length (Å) and $s$ the Pauling bond strength in valence units (v.u.). Taking into account the valence sum rule, the sum of the individual Mo–O bond strengths for a viable configuration of a Mo oxide species should equal to six. Equations (1) and (2) are valid for Mo–O stretching frequencies only (at best ⩾600 cm$^{-1}$). This approach is based on the diatomic approximation, which is necessary for justifying the direct relationship between metal–oxygen bond lengths and Raman stretching frequencies. Thus, to a first approximation, the Raman spectrum is simulated by a superposition of the stretching frequencies from an assembly of M–O diatomic oscillators [41]. As an example, we can calculate the bond lengths

and bond orders from the observed vibrational frequencies for the surface $MoO_x$ species of the 5MoAl sample. In case that the isolated molybdate has the monooxo configuration (CN = 5, Fig. 3B), the sum of v.u. remaining for the four Mo–O–Al anchoring bonds is 4.07 (after considering 1.93 v.u. resulting from Eqs. (1) and (2) for the 996 $cm^{-1}$ Mo=O band), resulting in a bond order of 1.02 for each Mo–O(–Al). Similarly, in the case of the dioxo configuration (CN = 4, Fig. 3A) we obtain a bond order of 1.07 for each Mo–O bond along the anchoring bridges. Eq. (1) then provides an estimate for the position of the Raman band due to Mo–O along Mo–O–Al for the configurations Figs. 3A and 3B as occurring in the range 675–690 $cm^{-1}$. This is quite close to the observed Raman band at ∼635 $cm^{-1}$ (inset Fig. 2) and supports the band assignments provided above.

Likewise, by addressing the case of a unit internal to a polymeric chain (with one short Mo=O, two bridging Mo–O–Mo to neighboring units and two Mo–O–Al anchoring bonds, CN = 5), we obtain 0.56 v.u. for each Mo–O along the anchoring bridges. It therefore turns out that, as shown also for $V_2O_5/TiO_2$ and $V_2O_5/ZrO_2$ catalysts [6], there are significant variations in bond strengths between anchoring bonds of isolated and polymeric units, the latter ones possessing weaker Mo–O bonds along the anchoring bridges. With increase in loading, polymeric species dominate and the weak 635 $cm^{-1}$ (assigned to isolated surface species) disappears. It should be pointed out that the above analysis assumes that the literature assignments for the Raman data are correct; recently, the V–O–V band assignment has been challenged for supported vanadia catalysts with the proposal of the "umbrella" model [42]. Finally, it should be pointed out that the above procedure (based on Eqs. (1) and (2)) adopting the diatomic approach is a simplifying one and constitutes only a good approximation; however this model provides a platform for discussing the viability of assignments and configurations.

### 3.2. Operando Raman spectra of catalysts during ethane ODH reaction conditions

The spectral and catalytic behavior of the catalysts under steady state ethane ODH conditions were first studied as a function of temperature (in the range 420–540 °C) at constant residence time ($W/F = 0.28$ g s/$cm^3$). The Raman spectra recorded under ethane ODH conditions for all catalysts at 540 °C are shown in Fig. 4 and the corresponding catalytic data recorded simultaneously are listed in Table 3.

For the 10MoAl and 15MoAl catalysts (spectra a and b in Fig. 4), the Mo=O band at ∼1000 $cm^{-1}$ drops in intensity and broadens under reaction conditions compared with the corresponding spectra obtained under $O_2$. The Mo–O–Mo broad band for the same samples now appears at ∼850 $cm^{-1}$, that is, with a 10–20 $cm^{-1}$ red shift compared with the oxidized catalysts. Moreover, the intensity of the Mo–O–Mo band appears to have increased for the 15MoAl sample relative to the intensity of the Mo=O band under reaction conditions. Furthermore, a new weak band at ∼760 $cm^{-1}$ appears and gains in intensity on going from 10MoAl (Fig. 4a) to 15MoAl (Fig. 4b). It appears that the decreased intensity of the Mo=O band (reflecting the loss of Mo(VI) sites due to reduction) is related to the appearance of the 760-$cm^{-1}$ band (with increasing intensity on going from spectrum a to b (Fig. 4)) and to the shift of the Mo–O–Mo band to ∼850 $cm^{-1}$. By switching the feed gas to pure $O_2$, the spectral characteristics of the oxidized catalysts (i.e., band positions and relative intensities) are reinstated. Evidently, the bands at 760 and 850 $cm^{-1}$ manifest the formation of partially reduced Mo surface oxide species. It has been reported that bands due to reduced Mo oxide species are readily observed in the Raman spectrum (e.g., under methanol oxidation conditions) [15,43], and the most prominent bands due to such species were observed at 840 and 760 $cm^{-1}$ [43]. It has also been reported that the reduction of Mo proceeds gradually, with the formation of a reduced $Mo^{5+}$–OH species as a first step and a $Mo^{x}$–O–$Mo^{5+}$ pair ($x = +5$ or $+4$) in a subsequent reduction step [44]. Finally, the red shift and broadening of the

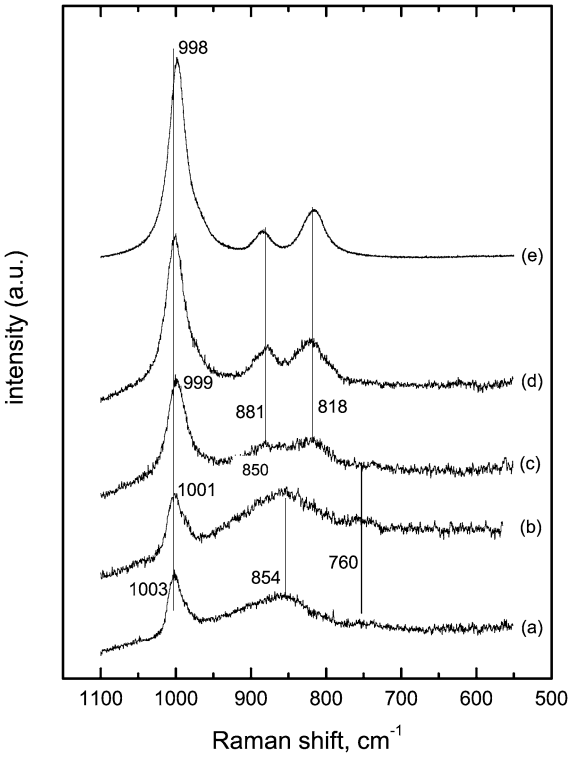


Fig. 4. Raman spectra of catalysts obtained under $C_2H_6/O_2$/He during ethane ODH at 540 °C: (a) 10MoAl; (b) 15MoAl; (c) 20MoAl; (d) 30MoAl; and (e) $Al_2(MoO_4)_3$. $W/F = 0.28$ g s/$cm^3$. Recording parameters: see Fig. 2 caption.

Table 3
Ethane conversion (%), yield to ethylene (%) and selectivity (%) to reaction products for all catalysts corresponding to measurements performed simultaneously with the recording of the Raman spectra shown in Fig. 4. $W/F = 0.28$ g s/$cm^3$

| Catalyst | Conversion (%) | $C_2H_4$ yield (%) | Selectivity (%) | | |
|---|---|---|---|---|---|
| | | | $C_2H_4$ | CO | $CO_2$ |
| $Al_2O_3$ | 21.1 | 2.1 | 10.2 | 43.9 | 45.9 |
| 5MoAl | 7.0 | 3.5 | 51.0 | 32.2 | 16.8 |
| 10MoAl | 9.7 | 7.0 | 72.5 | 20.9 | 6.6 |
| 15MoAl | 19.7 | 13.9 | 70.2 | 25.8 | 3.9 |
| 20MoAl | 21.6 | 15.2 | 72.5 | 24.3 | 3.2 |
| 30MoAl | 15.8 | 12.1 | 77.0 | 20.4 | 2.6 |

~1000-cm$^{-1}$ Mo=O band are attributed to perturbations from surface reaction intermediates, such as weakly bound surface ethoxides [45].

The spectrum of the 20MoAl catalyst (Fig. 4c) under reaction conditions is characterized by predominance of the $Al_2(MoO_4)_3$ bands. The absence of features due to dispersed fully oxidized species and of the 760- and 850-cm$^{-1}$ bands assigned to reduced Mo oxide species suggests a deeper reduction to lower valence states that do not give rise to Raman active modes. Thus, with increasing loading, deeper reduction of surface $MoO_x$ occurs, whereas the $Al_2(MoO_4)_3$ phase appears unaffected under the studied conditions (Fig. 4e).

Table 3 gives the catalytic activity data obtained for all samples studied and for the support at 540 °C and $W/F = 0.28$ g s/cm$^3$. It is seen the $Al_2O_3$ support exhibits measurable catalytic activity but poor selectivity to ethylene and should be expected to contribute to the reactivity of the samples with coverage below the monolayer. Measurable catalytic activity for $Al_2O_3$ support has also been observed for the methanol oxidation reaction [43].

The data in Table 3 show that the conversion of ethane and the yield to ethylene increase with increasing molybdena loading and reach maximum values for the 20MoAl sample. The selectivity to $C_2H_4$ is low for the 5MoAl catalyst (~50%) and generally slightly >70% for all catalysts with higher $MoO_3$ content. Moreover, the selectivity to $CO_2$ is rapidly reduced with increasing $MoO_3$ content. Thus, at low loadings when uncovered $Al_2O_3$ is available, conversion to $CO_x$ (particularly $CO_2$) is higher. The formation of dispersed molybdates at increasing loadings favors the selective activation of ethane.

### 3.3. Catalytic activity and selectivity

#### 3.3.1. Effects of temperature and residence time

Fig. 5 shows the dependence of ethane conversion on temperature (in the range of 420–540 °C) at a fixed residence time, $W/F = 0.28$ g s/cm$^3$. Ethane conversion increases with loading and goes through a maximum for 20MoAl at all temperatures. Fig. 6 shows the dependence of ethane conversion on residence time ($W/F$) at 540 °C. Ethane conversion increases with increasing $W/F$ for all samples. Moreover, ethane conversion increases with loading up to 20 wt% and then drops for 30MoAl. The 15MoAl and 20MoAl samples with $n_s$ close to the monolayer limit (~5 Mo/nm$^2$) have higher ethane conversions in the temperature and $W/F$ ranges studied.

Fig. 7 shows that ethylene selectivity decreases with increasing ethane conversion for all catalysts examined, in agreement with the trends generally observed for alkane ODH over supported metal oxide catalysts [6–8,23,39,46–49]. Selectivity is low for the 5MoAl sample and increases significantly for 10MoAl and 15MoAl, and remains unaffected by catalyst composition. This is seen more clearly in Fig. 8, which plots the initial (at ~6% ethane conversion) selectivities to $C_2H_4$ and to $CO_x$ versus $n_s$ (Mo/nm$^2$). Selectivity to $C_2H_4$ initially increases with increasing Mo surface density and attains a ~90% value for $n_s$ of > ~4 Mo/nm$^2$. Beyond the monolayer limit, the selectivity is independent on loading, being controlled by the

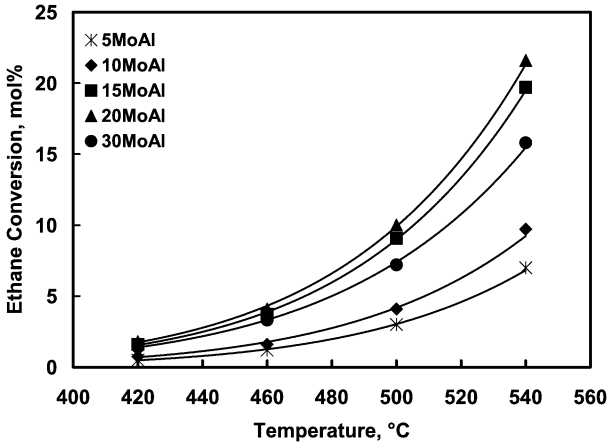


Fig. 5. Ethane conversion as a function of temperature, for all catalysts. $W/F = 0.28$ g s/cm$^3$.

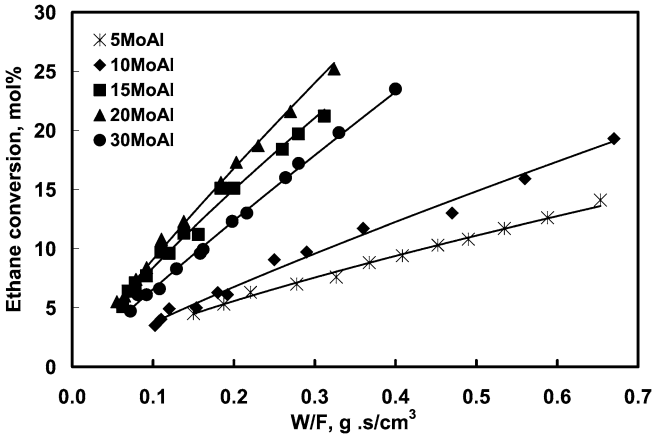


Fig. 6. Ethane conversion as a function of $W/F$ at 540 °C, for all catalysts.

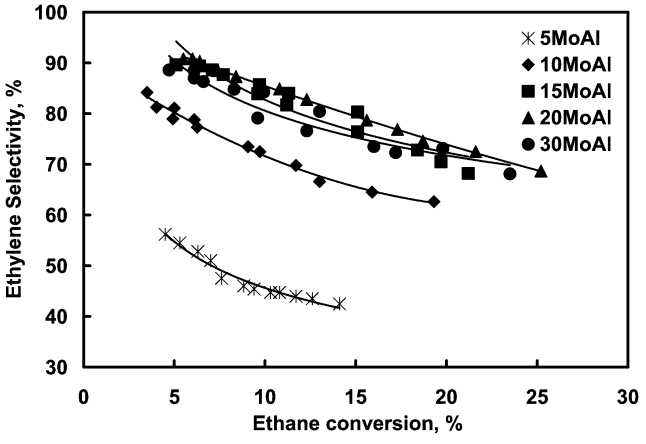


Fig. 7. Ethylene selectivity as a function of ethane conversion at 540 °C.

conversion level achieved. In addition, the $Al_2(MoO_4)_3$ phase is quite selective to $C_2H_4$ at low $C_2H_6$ conversion levels; runs performed with pure $Al_2(MoO_4)_3$ showed 99.8% selectivity to ethylene at ~3% ethane conversion. It appears that primary steps of $C_2H_6$ activation for $C_2H_4$ production are favored by the presence of $Al_2(MoO_4)_3$. Similar behavior has also been

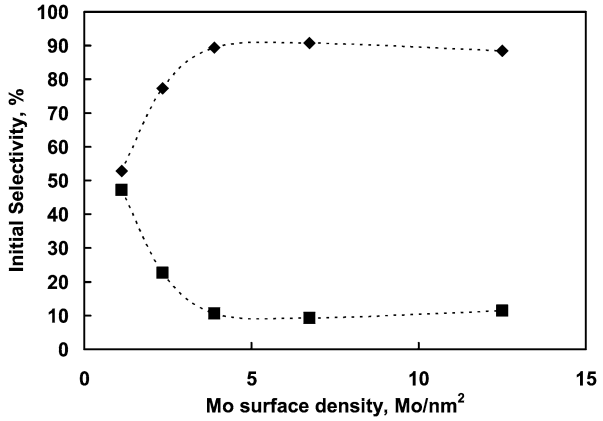


Fig. 8. Initial selectivity to $C_2H_4$ and $CO_x$ as a function of Mo surface density at 540 °C.

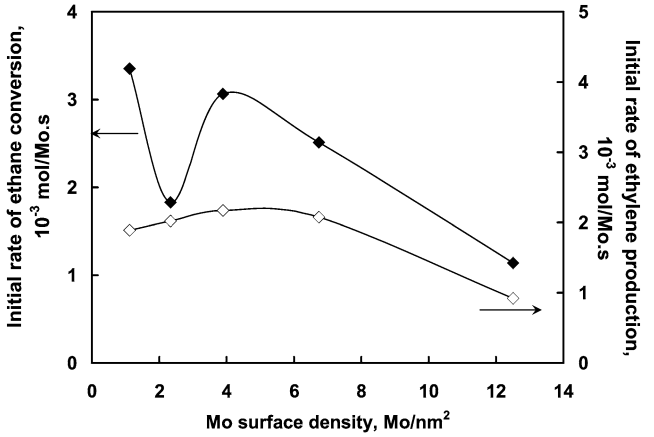


Fig. 9. Initial rate of $C_2H_6$ consumption and $C_2H_4$ production per Mo (TOF, $s^{-1}$) as a function of Mo surface density, $n_s$.

reported for $V_2O_5/ZrO_2$ catalysts for propane ODH, where the formation of crystalline $ZrV_2O_7$ allowed high initial propene selectivity [6].

Before closing this section, it is worth pointing out that the catalytic results shown in Figs. 5–7, obtained with the newly constructed reactor/Raman cell (Fig. 1), are in excellent agreement with previous results obtained with a "conventional" fixed-bed reactor for the same catalyst samples [8]. Therefore, the structure-activity relationships discussed below can be considered reliable.

### 3.3.2. *Effect of Mo surface density on the initial reaction rate*

Fig. 9 shows the initial ethane conversion and ethylene production rates normalized per Mo atom (TOF, $s^{-1}$) as a function of $n_s$ ($Mo/nm^2$). The high ethane conversion rate exhibited by the sample with the lowest $n_s$ (leading mainly to combustion products) is due to the high reactivity of the $Al_2O_3$ support, which remains uncovered. Ethane conversion rates normalized per Mo atom increase above $n_s = 2.3$ $Mo/nm^2$ and approach a maximum for a surface density corresponding to the monolayer, ∼5 $Mo/nm^2$ (Fig. 9). For $n_s > \sim 5$ $Mo/nm^2$, there is a systematic decrease in apparent turnover rate, attributed to the formation of bulk $Al_2(MoO_4)_3$, which reduces the accessibility of the $MoO_x$ dispersed species. However, an interesting trend is observed when the rate of ethylene production is plotted versus $n_s$ (Fig. 9). The ODH reactivity of the dispersed molybdena increases moderately as larger and more polymeric $MoO_x$ species are formed on the support surface, up to the limit of the polymolybdate monolayer, and then decreases.

Table 4 compares Raman characteristics, physicochemical properties, and reported trends for TOF values for $MoO_3/Al_2O_3$ catalysts examined in various catalytic reactions. The observed trend, according to which the TOF values initially increase with increasing $n_s$ and then decrease, is in agreement with the trends observed for the ODH of propane [39] and the selective oxidation of dimethyl ether [31] but contradicts the results for methanol oxidation [33], where an increasing trend in TOF is observed with increasing Mo surface density.

Fig. 10 shows initial $C_2H_4$ production rates normalized per sample surface area. The rate steadily increases as the $Al_2O_3$ surface is progressively covered by $MoO_x$ species and reaches a maximum value when approaching complete coverage of the support. Thus, increasing reactivity and better reducibility of $MoO_x$ structures with growing oxide domains count for the increase in turnover rates up to the monolayer limit in agreement with results of propane ODH [39]. Beyond that point, any additional Mo introduced becomes inaccessible, resulting in a decreased rate per Mo.

Table 4
Comparison between Raman stretching frequencies, physicochemical characteristics and trends in TOF values between $MoO_3/Al_2O_3$ supported catalysts

| | Ref. [39] | Ref. [31] | Ref. [32] | Ref. [33] | This work |
|---|---|---|---|---|---|
| Mo content | 0.4–11.3 $Mo/nm^2$ | ∼1–12 $Mo/nm^2$ | 4.2–13.9 wt% | 1–20 wt% | 1.1–12.5 $Mo/nm^2$ |
| Mo=O ($cm^{-1}$) | 1010 | 1001 | 996–1003 | 990, 1006 | 996–1004 |
| Mo–O–Mo ($cm^{-1}$) | Not reported | 865 | 853 | 865 | 850–870 |
| Coordination at | | | | | |
| Low coverage | Tetrahedral | | Monooxo octahedral | Tetrahedral | Tetrahedral + octahedral |
| High coverage | Octahedral | 2D oligomers | Octahedral, $Mo_7O_{24}^{6-}$ | Tetrahedral + octahedral | Octahedral |
| Calcination (K) | 773 | 773 | 773 | 773, 973 | 923 |
| Crystalline phases | $MoO_3$ | $MoO_3$ | | $MoO_3$ | $Al_2(MoO_4)_3$ |
| Trend for TOF with $n_s$ | Goes through a maximum[a] | Goes through a maximum[b] | – | Increase[c] | Goes through a maximum |

[a] For propane ODH.
[b] For the selective oxidation of dimethyl ether to formaldehyde.
[c] For the selective oxidation of methanol (catalytic results from Ref. [42]).

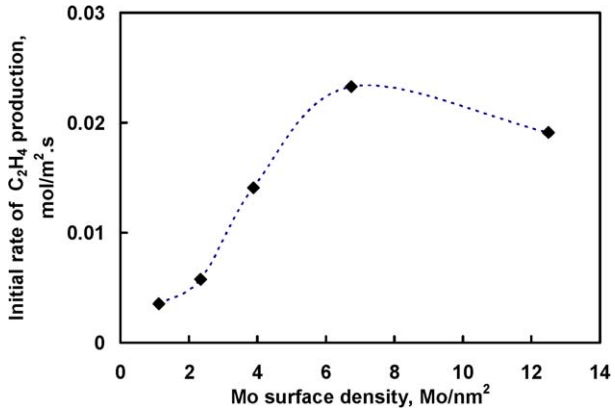


Fig. 10. Areal (per unit surface area) rate of $C_2H_4$ production as a function of Mo surface density at 540 °C.

### 3.3.3. Temperature and $W/F$ effects on the spectral behavior

Among the catalysts examined, the 20MoAl sample with $n_s$ slightly above the monolayer (6.7 Mo/nm$^2$) exhibited the best catalytic performance in terms of reactivity and ethylene yield for the temperature and $W/F$ ranges studied. Thus, for brevity, the temperature and $W/F$ effects on the spectral behavior are discussed only for this sample. Under dehydrated conditions, a temperature rise up to 540 °C results in broadening, moderate intensity loss, and a slight red shift of the strong ∼1000-cm$^{-1}$ Mo=O band (data not shown). Bands observed at 885, 820, and 382 cm$^{-1}$, due to bulk $Al_2(MoO_4)_3$, shift slightly to 878, 816, and 379 cm$^{-1}$, respectively, and progressively lose intensity with increasing temperature. The above spectral changes with temperature increase result from thermal broadening of the bands due to $Al_2(MoO_4)_3$ and increased optical absorption, leading to a decreased sampling depth for Raman spectroscopy and consequently to a loss of signal intensity [50].

Fig. 11 shows the dependence of Raman spectra under ethane ODH ($C_2H_6/O_2$) for the 20MoAl sample on temperature at fixed $W/F$ (spectra a–c) and on residence time ($W/F$) at constant temperature (spectra d–f). Whereas the effect of temperature was discussed earlier, the variation of residence time appears to have a significant effect (considering that the reaction operates in differential conditions) on the Raman spectra; for example, the ∼1000-cm$^{-1}$ Mo=O band loses intensity with increasing $W/F$, thereby reflecting the reduction of Mo(VI) sites to lower oxidation states.

Fig. 12 shows the rates (normalized per Mo) for $C_2H_4$ and $CO_x$ formation and the selectivity to $C_2H_4$ as functions of residence time ($W/F$) for the 20MoAl sample. Selectivity to $C_2H_4$ drops with increasing bed residence time (resulting in higher conversion), giving rise to higher CO selectivity, whereas $CO_2$ selectivity remains constant. Thus CO forms due to overoxidation of $C_2H_4$ produced at high conversions.

### 3.4. Structure–activity/selectivity relationships

Understanding the response of a catalyst surface to the reaction environment is a common goal in catalysis research. Understanding the transformation of the molecular structure (by, e.g., in situ Raman spectroscopy) of a catalyst when changing the surrounding environment is of direct relevance to the above goal. The combination of in situ Raman spectroscopy and activity measurements is a powerful strategy for deriving structure–activity relationships.

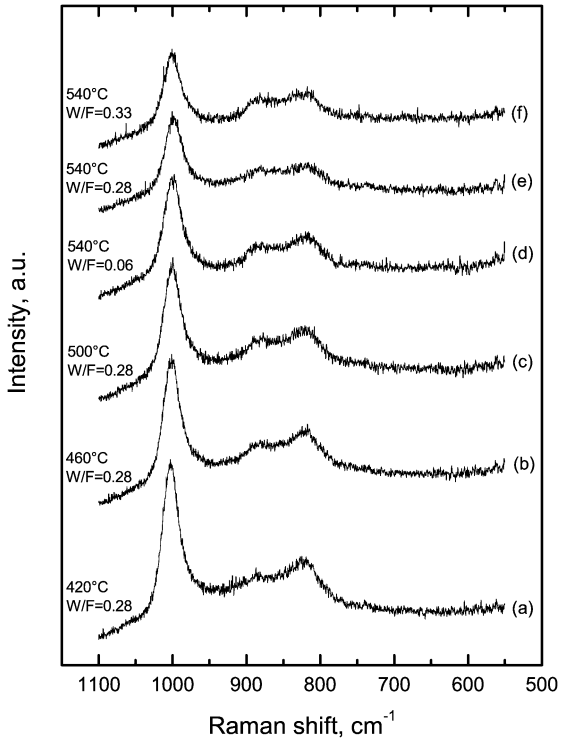


Fig. 11. Raman spectra of 20MoAl catalyst obtained under $C_2H_6/O_2$/He during ethane ODH as a function of temperature and $W/F$ as indicated by each spectrum. Recording parameters: see Fig. 2 caption.

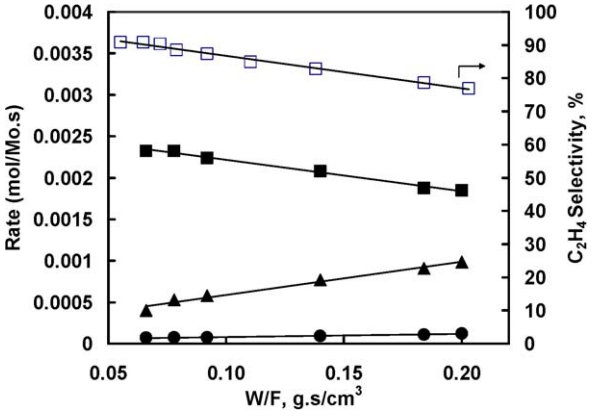


Fig. 12. Rates of $C_2H_4$, CO and $CO_2$ formation and $C_2H_4$ selectivity as a function of $W/F$ for 20MoAl catalyst at 540 °C.

There is a general consensus in literature that alkane ODH reactions proceed via a Mars van Krevelen redox-type reaction scheme involving lattice oxygen [10,37]. However, there is not a general agreement concerning which particular oxygen site is involved in the C–H bond activation. In the present study, the following $MoO_x$ surface species were found to exist on the support surface: (i) isolated $MoO_4$ and probably $MoO_5$ monomers (A and B in Fig. 3), (ii) surface polymolybdates (Fig. 3C and D) and (iii) bulk $Al_2(MoO_4)_3$. The various surface species include

different Mo–O bonding types and strengths. Thus, the critical oxygen involved in the active site for the ethane ODH reaction could in principle be involved in Mo=O terminal bonds, Mo–O–Mo bridging bonds or Mo–O–Al anchoring bonds of the surface metal oxide species. The roles of each of the above Mo–O bonds are examined below.

The band positions of terminal Mo=O and bridging Mo–O–Mo are independent of catalytic activity (TOF). For example, at 420 °C, the TOF value for the sample with $n_s = 3.9$ Mo/nm$^2$ ($2.4 \times 10^{-4}$ s$^{-1}$) is more than twice that for the sample with $n_s = 2.3$ Mo/nm$^2$ ($1.1 \times 10^{-4}$ s$^{-1}$), although the band positions for Mo=O and Mo–O–Mo are comparable for the two samples. Thus, it appears that the oxygen sites in the Mo=O and Mo–O–Mo bonds are not of critical importance for the activation of ethane. Previously, M=O (M = Mo,V) centers were not considered of critical importance for methanol oxidation reactions over $MoO_3/Al_2O_3$ catalysts [32,43] and for propane ODH over $V_2O_5/TiO_2$ and $V_2O_5/ZrO_2$ catalysts [6,51]. However, the reports do not converge, because it has also been reported that Mo=O bonds are active for C–H bond activation for the ODH of propane over $MoO_3/ZrO_2$ catalysts [37]. This was based on observation of weakening Mo=O bond strengths with correspondingly increasing catalytic activity.

A number of factors could govern to various extents the activity of molybdena/alumina catalysts for ethane ODH at coverages below monolayer. Such factors may include site reactivity/selectivity, site reducibility, and site availability. The eventual occurrence of different active sites (active phase heterogeneity)—each with its own selectivity—could make identification of the active site difficult. The observed monotonic increase of the catalyst reducibility with increasing Mo surface density [39] receives special attention. This could indicate a parallel increase in the active site availability. Below we attempt to correlate the activity per Mo (TOF) to the number of active sites per Mo on grounds of stable site selectivity, by assuming that the reactivity per site does not change with increasing surface density.

With reference to the observed trends in TOF (activity per Mo) versus $n_s$, one could state that on the basis of stable site reactivity, this trend should concur with the trend in the number of active sites per Mo. Therefore, the observed trend of TOF versus $n_s$ (i.e., passing through a maximum; see Fig. 9) excludes the Mo=O site from being the active site, because the number of such sites per Mo initially decreases on going from two Mo=O per Mo for the dioxo $MoO_4$ monomolybdate to one Mo=O per Mo with gradual enrichment of the surface with polymolybdates and eventually remains constant, because at high loadings there is one Mo=O per Mo. Even if the site reactivity varies with loading, we would expect to see monotonic behavior (i.e., a steady increase or a steady decrease), not the passage through a maximum as shown in Fig. 9.

Likewise, the oxygen site of Mo–O–Mo bridges can be eliminated as being of critical importance. As shown in the discussion pertaining to Fig. 2, the gradual increase in intensity of the broad band at 850–870 cm$^{-1}$ due to Mo–O–Mo relative to the ∼1000 cm$^{-1}$ Mo=O with increasing loading reveals a monotonic increase in the degree of polymerization, that is, with an increasing number of Mo–O–Mo bridges per Mo (from 0 for monomolybdates to 0.5 for a dimer, 0.65 for a trimer, etc.).

As pointed out earlier, ethane ODH rates appear to increase and then decrease moderately with Mo surface density. The evolution of the structural characteristics for the surface-dispersed $MoO_x$ species established by the Raman data produces an interesting trend for the number of Mo–O–Al anchoring bonds per Mo with increasing loading. It is evident from Fig. 3 that isolated $MoO_4$ species (Fig. 3A), which predominate at low loadings, have two terminal Mo=O bonds and two anchoring Mo–O–Al bonds per Mo atom. However, as $MoO_3$ loading increases, the surface of the support gradually becomes covered by polymeric species in chain-like arrangements, giving rise to an increasing population of dimers, trimers, and so on (Fig. 3C and D) with numbers of Mo–O–Al per Mo that initially increase and then moderately decrease. For instance, a $(MoO_x)_2$ dimer has 3 Mo–O–Al bonds per Mo, a trimeric $(MoO_x)_3$ has an average of ∼2.7 Mo–O–Al bonds per Mo, a tetrameric unit has 2.5 Mo–O–Al bonds per Mo, and so on. Thus, for any case, the increasing relative population of polymeric to monomeric $MoO_x$ species with increasing loading results in a parallel initial increase in the number of Mo–O–Al bonds per Mo atom, followed by a moderate decrease. Therefore, there are concurrence trends for TOF and the number of Mo–O–Al bonds per Mo as a function of increasing Mo oxide content, indicating the significance of these bonds for the ethane ODH reaction. The oxygen involved in Mo–O–support anchoring bonds has also been proposed previously as the critical site for the selective oxidation of methanol and for alkane ODH reactions [2,32,43].

To further strengthen the above conclusion, we examined the support effect by measuring the ethane ODH TOF over a $MoO_3/ZrO_2$ catalyst with $n_s = 1.7$ Mo/nm$^2$ at 420 °C. Although the Mo=O and Mo–O–Mo band positions were similar to the positions of the $MoO_3/Al_2O_3$ catalysts, a ∼20-fold increase in TOF was found. The foregoing observation points to the specific properties and types of the Mo–O–support anchors as being of importance for the activation of the C–H bond in ethane ODH.

## 4. Conclusion

The Raman spectra of the catalysts recorded under pure $O_2$ conditions reveal the existence of dispersed molybdena species on the surface of the $Al_2O_3$ support in various molecular configurations, depending on loading. In general, at low loadings, both monomeric species (most probably in dioxo configuration with CN = 4) and polymeric species in distorted octahedral configuration coexist on the support surface, whereas at higher $MoO_3$ loadings, incorporation of Mo to Mo–O–Mo bridging bonds results in a greater abundance of polymeric $MoO_x$ chains on the catalyst surface. Bulk $Al_2(MoO_4)_3$ is detected at Mo surface densities slightly above the theoretical monolayer. Under ethane ODH reaction conditions, the Raman spectra are indicative of the reduction of the surface $MoO_x$ species to lower valence states due to their participation in catalytic turnover; the extent of Mo reduction is found to increase with increasing

loading. The combination of the spectral characteristics of the catalysts and the catalytic activity and selectivity data collected simultaneously allows us to derive structure–activity relationships. The trend in ethane ODH rate per Mo versus $n_s$ (initial increase followed by a decrease) concurs with the trend in the number of Mo–O–Al bonds per Mo for the dispersed surface $MoO_x$ species with increasing $n_s$. The data indicate the significance of the anchoring Mo–O–Al bonds to the catalytically relevant reaction steps.

## Acknowledgments

Financial support from the European Social Fund (ESF), Operational Program for Educational and Vocational Training II (EPEAEK II), and particularly the IRAKLEITOS program is gratefully acknowledged.

## References

[1] F. Cavani, F. Trifiro, Catal. Today 24 (1995) 307.
[2] M.A. Banares, Catal. Today 51 (1999) 319.
[3] A.M. Beale, A.M.J. van der Eerden, K. Kervinen, M.A. Newton, B.M. Weckhuysen, Chem. Commun. (2005) 3015.
[4] E.A. Mamedov, V.C. Corberán, Appl. Catal. A 127 (1995) 1.
[5] T. Blasco, J.M. Lopez Nieto, Appl. Catal. A 157 (1997) 117.
[6] A. Christodoulakis, M. Machli, A.A. Lemonidou, S. Boghosian, J. Catal. 222 (2004) 293.
[7] A.A. Lemonidou, L. Nalbandian, I.A. Vasalos, Catal. Today 61 (2000) 333.
[8] E. Heracleous, A.F. Lee, I.A. Vasalos, A.A. Lemonidou, Catal. Lett. 88 (2003) 47.
[9] M.C. Abello, M.F. Gomez, O. Ferretti, Appl. Catal. A 207 (2001) 421.
[10] K. Chen, A.T. Bell, E. Iglesia, J. Phys. Chem. B 106 (2000) 1292.
[11] E. Heracleous, J. Vakros, A.A. Lemonidou, Ch. Kordulis, Catal. Today 91–92 (2004) 289.
[12] L. Wang, W.K. Hall, J. Catal. 83 (1983) 242.
[13] F.R. Brown, L.E. Makovsky, K.H. Rhee, J. Catal. 50 (1977) 162.
[14] I.E. Wachs, Catal. Today 27 (1996) 437.
[15] G. Mestl, J. Mol. Catal. A Chem. 158 (2000) 45.
[16] I.E. Wachs, Top. Catal. 8 (1999) 57.
[17] A. Christodoulakis, S. Boghosian, J. Catal. 215 (2003) 139.
[18] I. Giakoumelou, V. Parvulescu, S. Boghosian, J. Catal. 225 (2004) 337.
[19] I. Giakoumelou, Ch. Fountzoula, Ch. Kordulis, S. Boghosian, J. Catal. 239 (2006) 1.
[20] Y.C. Xie, Y.Q. Tang, Adv. Catal. 37 (1990) 1.
[21] J.A. Bergwerff, T. Visser, B.R.G. Leliveld, B.D. Rossenaar, K.P. de Jong, B.M. Weckhuysen, J. Am. Chem. Soc. 126 (2004) 14548.
[22] B.M. Weckhuysen, Chem. Commun. (2002) 97.
[23] G.G. Cortez, M.A. Banares, J. Catal. 209 (2002) 197.
[24] Operando spectroscopy: fundamental and technical aspects of spectroscopy of catalysts under working conditions, Phys. Chem. Chem. Phys. 5 (20) (2003) (Special issue).
[25] M.A. Banares, Catal. Today 100 (2005) 71.
[26] I.E. Wachs, Catal. Today 100 (2005) 79.
[27] S. Xie, K. Chen, A.T. Bell, E. Iglesia, J. Phys. Chem. B 104 (2000) 10059.
[28] Z. Vit, M. Zdrazil, J. Catal. 171 (1997) 305.
[29] G. Mestl, T.K.K. Srinivasan, Catal. Rev. Sci. Eng. 40 (4) (1998) 451.
[30] H. Jezlorowski, H. Knözinger, J. Phys. Chem. 83 (1979) 1166.
[31] H. Liu, P. Cheung, E. Iglesia, J. Catal. 217 (2003) 222.
[32] D.S. Kim, I.E. Wachs, K. Segawa, J. Catal. 146 (1994) 268.
[33] H. Hu, I.E. Wachs, S.R. Bare, J. Phys. Chem. 99 (1995) 10897.
[34] B.M. Weckhuysen, J.-M. Jehng, I.E. Wachs, J. Phys. Chem. B 104 (2000) 7382.
[35] G. Busca, J. Raman Spectrosc. 33 (2002) 348.
[36] K. Nakamoto, in: Infrared and Raman Spectra of Inorganic and Coordination Compounds, fourth ed., Wiley–Interscience, New York, 1986, pp. 142, 149.
[37] K. Chen, S. Xie, E. Iglesia, A.T. Bell, J. Catal. 189 (2000) 421.
[38] M.A. Vuurman, I.E. Wachs, J. Phys. Chem. 96 (1992) 5008.
[39] K. Chen, S. Xie, A.T. Bell, E. Iglesia, J. Catal. 198 (2001) 232.
[40] F.D. Hardcastle, I.E. Wachs, J. Raman Spectrosc. 21 (1990) 683.
[41] F.D. Hardcastle, I.E. Wachs, J. Phys. Chem. 95 (1991) 5031.
[42] J.N.J. van Lingen, O.L.J. Gijzeman, B.M. Weckhuysen, J.H. van Lenthe, J. Catal. 239 (2006) 34.
[43] H. Hu, I.E. Wachs, J. Phys. Chem. 99 (1995) 10911.
[44] E. Payen, S. Kasztelan, S. Houssenbay, R. Szymanski, J. Grimblot, J. Phys. Chem. 93 (1989) 6501.
[45] E. Heracleous, A.A. Lemonidou, J.A. Lercher, Appl. Catal. A 264 (2004) 73.
[46] K. Chen, S. Xie, A.T. Bell, E. Iglesia, J. Catal. 195 (2000) 244.
[47] C.L. Pieck, M.A. Banares, J.L.G. Fierro, J. Catal. 224 (2004) 1.
[48] M.C. Abello, M.F. Gomez, M. Casella, O.A. Ferretti, M.A. Banares, J.L.G. Fierro, Appl. Catal. A 251 (2003) 435.
[49] R.J. López, N.S. Godjayena, V.C. Corberán, J.L.G. Fierro, E.A. Mamedov, Appl. Catal. A 124 (1995) 281.
[50] S. Xie, E. Iglesia, A.T. Bell, J. Phys. Chem. B 105 (2001) 5144.
[51] B.M. Weckhuysen, D.E. Keller, Catal. Today 78 (2003) 25.